Available online at www.sciencedirect.com

ScienceDirect

Advances in Space Research xxx (xxxx) xxx

ADVANCES IN SPACE RESEARCH (a COSPAR publication)

www.elsevier.com/locate/asr

Monitoring of local deformations and reservoir water level for a gravity type dam based on GPS observations

J. Rene Vazquez-Ontiveros [a], Carlos A. Martinez-Felix [a,*], G. Esteban Vazquez-Becerra [a] J. Ramon Gaxiola-Camacho [b], Angela Melgarejo-Morales [a], Jorge Padilla-Velazco [a]

[a] Department of Earth and Space Sciences, Autonomous University of Sinaloa, Culiacan, Sinaloa 80040, Mexico
[b] Department of Civil Engineering, Autonomous University of Sinaloa, Culiacan, Sinaloa, Mexico

Received 9 May 2021; received in revised form 12 September 2021; accepted 16 September 2021

Abstract

In order to find a possible relation between the reservoir level and the deformation of the Sanalona dam, the horizontal and vertical displacements for a period of 3.5 years using GPS observations were calculated. The GAMIT/GLOBK scientific software was used for the relative processing of GPS observations and annual speeds over the dam of −6.77 mm/yr, −9.95 mm/yr and −1.62 mm/yr were calculated for the N, E and U components, respectively. In addition, the GNSS reflectometry inversion technique was applied to determine the daily reservoir level of the dam, the values obtained were compared with the real reference values of graduated rulers in situ. The GNSS-R achieved a correlation coefficient (ρ) of 0.97 with a root-mean-square error (RMSE) of 1.36 m and a regression slope of 0.932 m/m. The deformation in the x^{Dam} component obtained a greater relation with the reservoir level due to the thrust force generated on the crest. The results demonstrate that it is possible to use a GPS antenna to carry out two monitoring processes together on a dam: (1) determination of displacements and (2) calculation of reservoir level.

Keywords: Gravity-type dams; Horizontal and vertical displacements; GNSS-R inversion; Reservoir level; Dam deformation

1. Introduction

Dams play an essential role in the socio-economic development of a country due to their capacity to store water for human consumption, irrigation of large areas of agricultural fields, flood control and hydroelectric energy production, to name a few (Yigit et al., 2016; Yavaşoğlu et al., 2018). On the other hand, dams are in constant interaction with the environment and with hydraulic and geomechanical factors which in most of the cases induce horizontal and vertical displacements on the structure of the crest. When displacements exceed the critical limit, catastrophic damage may occur. For example, in 1975 the Bangiao dam, located in Henan province in central China, collapsed as a consequence of a typhoon impact. This caused that millions of people lost their homes and a death toll of more than 26,000 was documented (Yang et al., 2017). Another disaster occurred in 1985 in northern Italy where the collapse of the Stava dam caused that 270 people lost their lives (Graham, 1999). Therefore, one of the main reasons for monitor the structural response of dams is because although dams are necessary for human society these represent a potential risk. Thus, it is important to monitor its structural response in order to detect anomalies that could be an indicator of potential failure

* Corresponding author.
E-mail addresses: jesusrene@uas.edu.mx (J.R. Vazquez-Ontiveros), carlosmartinez@uas.edu.mx (C.A. Martinez-Felix), gvazquez@uas.edu.mx (G.E. Vazquez-Becerra), jrgaxiola@uas.edu.mx (J.R. Gaxiola-Camacho), angelamelgarejo@uas.edu.mx (A. Melgarejo-Morales).

https://doi.org/10.1016/j.asr.2021.09.018
0273-1177/

and thereby be able to offer early warnings for appropriate corrective actions (Bukenya et al., 2014; González-Aguilera et al., 2008; Konakoglu et al., 2020; Xi et al., 2018).

In general, dam monitoring consists mainly on surveillance, instrumentation, data acquisition, evaluation, analysis, management and decision-making based on the extracted results (FEMA, 2015). Therefore, different structural monitoring studies on concrete dams have been carried out considering geodetic and geotechnical methods (Ehiorobo and Irughe-Ehigiator, 2011; Kalkan, 2014; Yigit et al., 2016). For instance, Guler et al., (2006), using the Karlsruhe geodetic method, evaluated the surface displacements of the Alibey earth dam located on Istanbul, the results obtained with the geodetic method were compared with respect to those obtained via finite element model (FEM) analysis and both were in concordance. Moreover, a three-dimensional (3D) terrestrial laser scanner (TLS) for structural monitoring of dams was tested (González-Aguilera et al., 2008). They concluded that a TLS alone is not sufficient to monitor the structural control of dams since it is not possible to monitor the same point at different times of measurement. Also, the implementation of what is considered as the first GPS deformation monitoring system for dams was presented by Hudnut and Behr (1998). In specific, the implementation of a system of continuous monitoring GPS stations to monitor, since 1995, the displacements of the Pacoima dam located in California, USA. The results showed displacements downstream of the dam center during the autumn and winter followed by upstream deviations during the spring and summer, displacements were in the order of 20 mm. Some of the advantages of Global Navigation Satellite Systems (GNSS) over traditional surveying methods such as leveling and trilateration are that GNSS provides stable and continuous observations throughout the year regardless of weather conditions (Xiao et al., 2019). Another study was carried out by Yigit et al., (2016), where the dynamic behavior of the Ermenek dam was studied through conventional geodetic measurements and the FEM analysis during the initial filling period. The results showed that the displacement responses of the dam were related to temperature variations and the linear increase in the level of the reservoir. Additionaly, Acosta et al., (2018) studied the behavior of an earth-fill dam and analyzed the deformations obtained by high-precision geodetic techniques and GNSS using FEM to determine the reference displacements. In the aforementioned study, seven GNSS measurements campaigns were carried out for some months of years 2008 to 2016. Then, a comparative evaluation between the predicted FEM results and the observed deformations demonstrated differences of 20 and 6 cm on the horizontal and vertical displacements of the dam crest, respectively.

The reservoir level of a dam is one of the most important parameters to monitor along with three-dimensional displacements (Pytharouli and Stiros, 2005). The high levels of the reservoir of a dam can influence the local deformations of the crest due to the thrust force generated (Yigit et al., 2016). Reservoir levels are traditionally recorded using measuring stations (graduated ruler). However, stations can be affected by storms or even systematic errors (Ridolfi and Manciola, 2018). As an alternative, new techniques have been developed for water level measurements such as satellite images, drone photography and GNSS reflectometry (Munyaneza et al., 2009; Ridolfi and Manciola, 2018; Xi et al., 2018; Song et al., 2019). Thus, the need to study the behavior of dam reservoirs through continuous and precise structural monitoring techniques is well-established. The latter lead to an opportunity of implement a technique previously tested to measure snow depth and sea level: the GNSS-R inversion technique, but this time with the aim of monitor the reservoir level, regardless the environmental conditions.

In the background literature, different methodologies for water level retrievals using GNSS-R have been proposed. First, the phase-difference analysis technique which measures the discrepancy in terms of phase of the direct and reflected GNSS signals in order to obtain the direction length variation (Löfgren et al., 2011a,b). However, this technique demands the use of two antennas. In specific, one antenna is pointed to the zenith in order to receive direct signals while the second antenna is pointed to the nadir to receive reflected signals. Second, the Signal-to-Noise Ratio (SNR)-based analysis technique which evaluates the SNR pattern involving the interference of the direct and reflected GNSS signals (Bilich et al., 2007; Larson et al., 2013). According to Joseph (2010), the SNR or carrier-to-noise-density ratio (C/N_0) is commonly recorded by GPS receivers denoting the ratio between the signal or carrier power C and the noise power in terms of spectral density N_0 in units of decibel-hertz (dB-Hz). Furthermore, the SNR data is available in the RINEX observation files as observables S1 for L1 C/A signal, S2 for L2 signal and if available, S5 for the relatively new L5 signal. The SNR-based technique analyze the spectral density through the Lomb-Scargle periodogram (LSP) where its respective dominant frequency can be used as a reflector height (Larson et al., 2017, 2013; Löfgren et al., 2014). The latter has the advantage that only one antenna is required in order to compute water level retrievals as well as better performance during high wind conditions and in obtaining other sea-state parameters such as significant wave height (SWH), which is commonly provided by altimetry missions (Cipollini et al., 2017; Soulat et al., 2004). Nevertheless, it is worth mentioning that the phase-difference analysis has a relatively higher precision compared to the basic SNR-based technique (Löfgren and Haas, 2014). In general, spaceborne technology represent a proficient tool to detect and study phenomena that is likely to cause negative effects on a dam's structure over the years. Hence, this article aims to determine the horizontal and vertical displacements of the Sanalona dam along to its possible correlation with the reservoir level, calculated using the GNSS-R inversion technique through the collection of a set of GNSS spatial data.

The paper is organized as follows: The processing of GPS observations to find the displacements and the GNSS reflectometry technique is documented in Section 2. In Section 3 the characteristics of the Sanalona dam are described. Finally, the results and conclusions are mentioned in Sections 4 and 5, respectively.

2. Processing strategy

2.1. Monitoring of displacements on the Sanalona dam with GPS measurements

2.1.1. Data acquisition

In June 2016 the National Seismological Service (SSN as its acronym in Spanish) of Mexico installed a continuous monitoring GPS station on the Sanalona dam for seismicity studies, named SSIG. Its geographic coordinates are 24° 48′59.14″N, 107°8′41.65″W and its elevation is 130.6 m. This GPS station comprises a TRIMBLE NETRS receiver and a TRM57971.00 antenna, the sampling frequency is 1 Hz and it tracks only the GPS constellation. In relation to the data acquisition, these were provided by the National Seismological Service, specifically from June 2016 to December 2019 in a binary format and with a sampling rate of 1 Hz. On the other hand, the TEQC software (Estey and Meertens, 1999) was used in a UNIX script to convert the binary files to RINEX (Receiver INdependent EXchange) format and decimate them to the same sample rate of the stations defining the reference frame (30 s). The GPS antenna is located on the roof of a concrete structure that protects the seismic instruments and it is localized on the crest of the dam. Therefore, the possible displacements on the dam caused by the pushing force of the water will also be reflected on the structure. Moreover, the location of the antenna allowed the multipath errors to be reduced, improving the final precision. Fig. 1a shows the location of the GPS station on the dam, and Fig. 1b shows the topography that defines the dam. Due the remote access where SSIG station is installed some technical problems related with the data transfer belonging to the evaluation period of this research occurred.

2.1.2. GPS data processing

The GPS data were analyzed using GAMIT/GLOBK scientific software (Alcay et al., 2019; Herring et al., 2010) and in order to stablish the reference frame 12 GNSS stations for continuous monitoring belonging to the IGS network were used. The minimum and maximum lengths of the baselines between the reference stations and the SSIG station are 514 km and 1860 km, respectively. The observation files were downloaded from June 24, 2016 to December 20, 2019 which corresponds to a measurement period greater than 3.5 years. In a global reference frame and in order to obtain a low speed bias, the minimum recommended period for the analysis of the coordinates is 2.5 years (Blewitt and Lavallée, 2002), the selected period exceeds this. Fig. 2 shows the GNSS stations used for the establishment of the reference frame. Also, Table 1 summarizes the processing parameters used in this study. The time series generated by GAMIT/GLOBK were edited with the tsview tool developed by Herring (2003) this in order to remove the trend of the time series and eliminate outliers.

The coordinates resulting from the GAMIT/GLOBK process were calculated in the ECEF (Earth-Centred Earth-Fixed) cartesian coordinates system. However, its direct use is not suitable for interpreting the horizontal and vertical displacements of the dam structure due to its origin (Yigit, 2016). Therefore, to solve this problem the ECEF (X, Y, and Z) coordinates were transformed to the NEU (North, East, Up) topocentric coordinate system. The transformation was performed automatically by GAMIT/GLOBK and the NEU coordinates can be found in the output files together with the ECEF and geodetic coordinates. On the other hand, the N and E axes of the topocentric coordinates were oriented towards the North and East directions, respectively. Thus, the horizontal displacements derived from the GPS measurements of the dam were represented on the N and E axes. Consequently, the NEU coordinate system and the coordinate axes of the dam differ; this can be seen in Fig. 3. Therefore, the horizontal topocentric coordinates (N and E) were transformed to local coordinates of the dam (x^{Dam} and y^{Dam}) using the following equations (Yigit, 2016):

Fig. 1. (a) GPS antenna location and (b) topography that defines the dam.

Fig. 2. GNSS reference stations which defined the reference frame for GAMIT/GLOBK processing.

Table 1
GAMIT/GLOBK processing parameters.

GNSS system	GPS
Epoch interval	30 s
Ephemerides	IGS final orbits
Elevation mask	10°
Antex file	Igs14.atx
Code differential bias	Update DCB file
Ambiguity resolution method	Wide Lane and Narrow Lane
Observations	Code + Carrier phase
Tropospheric models	GPT3_1 model
Ionospheric model	Global ionospheric
Ocean tide model	FES2014b
Reference frame	Igb14
Adjustment method	Kalman filter

$$x^{Dam} = N\cos(\beta) + E\sin(\beta)$$
$$y^{Dam} = -N\sin(\beta) + E\cos(\beta) \quad (1)$$

where β is the rotation angle between the topocentric coordinates and the coordinates of the dam. Considering that the angle β is the heading of the quadrant of the dam's reference line due that the x^{Dam}-axis is perpendicular to the y^{Dam}-axis, which in turn is oriented towards the reference stations. So, β was calculated using the coordinates of the reference stations in order to determine the orientation of the y^{Dam}-axis. Finally, the displacements measured on the dam were represented in local coordinates of the structure, where the crest represents the y^{Dam}-axis.

Find the effect of the reservoir level with the deformations of the dam was one of the objectives of this research. Hence, we applied the moving average filter with a window of 100 samples to smooth the behavior and reduce the dispersion of the time series that correspond to the daily displacements in the horizontal (x^{Dam} and y^{Dam}) and vertical (U) components. Thereby, the time series present a behavior that resembles the real displacements of the structure. In general, the moving average filter is the simplest smoothing method; it consists of a window that replaces each spectral point with the average of the surrounding points within the smoothing window. Subsequently, the window is moved one point and the calculation is repeated for the new point. The general shape of the filter was simplified as given in Equation (2) (Guzman-Acevedo et al., 2019; Vazquez-ontiveros et al., 2021):

$$y(i) = \frac{1}{L}\sum_{j=0}^{L-1} x(i+j) \quad (2)$$

where x() is the input signal (x^{Dam}, y^{Dam} and U), y() is the output signal and L is the size of the window.

2.2. GNSS-R data processing

In order to improve water level retrievals, based on the SNR signals, Nievinski and Larson (2014a) proposed a forward and inverse modeling of SNR data which is based on a statistically rigorous inverse model that handles internally a physically forward model to retrieve residuals and obtain biases that can be translated into reflector height. This inversion technique was first tested for measuring snow depth applications (Nievinski and Larson, 2014b; Tabibi et al., 2017) and later for coastal sea level monitoring (Geremia-Nievinski et al., 2020). For water level studies, the inversion technique reported an improvement in precision terms against the basic SNR-LSP analysis (Geremia-Nievinski et al., 2020; Strandberg et al., 2016). Hence,

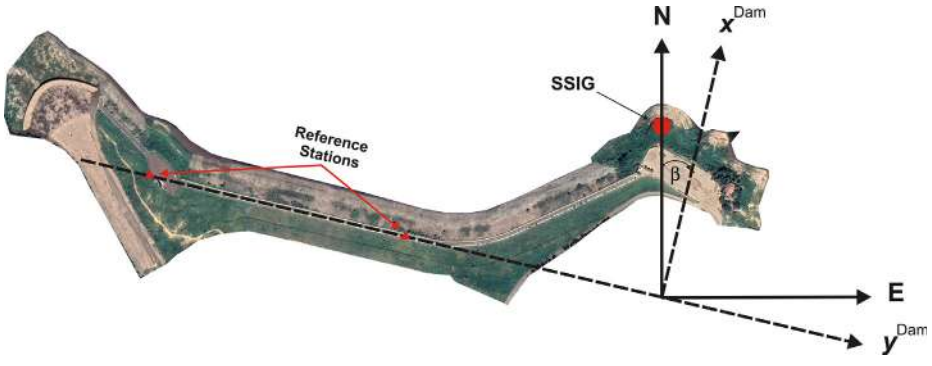

Fig. 3. Orientation of the dam coordinate axes and GPS measurements.

due the geodetic station SSIG incorporates only one pair of antenna/receiver and taking into advantage the latest improvements in SNR data processing, the inversion technique to retrieve the dam water level measurement was selected.

As was stated above, the inversion technique is composed of two models, one physical forward model and one statistical inverse model. In the forward model, the SNR is represented as the ratio between the signal noise P_n and the signal power P_s, where the latter is composed by the sum of its respective direct P_d and reflected powers P_r as well as the direct ϕ_d and reflected ϕ_r phases, as follows: $SNR = P_s/P_n$. Therefore, the physical model in SNR terms can be decomposed into the sum of a trend $tSNR$ and detrended interference fringes $dSNR$ as $SNR = tSNR + dSNR$, in this turn, each term can be defined as (Nievinski and Larson, 2014a):

$$tSNR = (P_d + P_r)/P_n = (P_d^R G_d^R + P_d^R |X|^2 S^2)/P_n \quad (3)$$

$$dSNR = 2\sqrt{P_d}\sqrt{P_r}P_n^{-1}\cos\phi_i \quad (4)$$

From the trend SNR, P_d^R is the right-hand circularly polarized (RHCP) power component, G_d^R is the direct antenna gain which is in function of the satellite direction, X is the composition of the surface reflection coefficients in function of the RHCP and Left-hand circularly polarized (LHCP) components and S is the attenuation factor of the coherent power. In the detrended SNR, ϕ_i is the interferometric phase which is formulated as the difference between the reflected and direct phase $\phi_i = \phi_r - \phi_d$. In this turn, ϕ_i is a function of the geometric component produced by the propagation delay of both reflected and direct path. Therefore, an approach of the interferometric phase corresponds to $\phi_i \approx (2\pi/\lambda)H\sin e$, where λ is the wavelength, i.e., 19.05 cm for the GPS L1 frequency signal, H is the reflector height and e is the satellite elevation angle with respect to the antenna. The parameters involved in the physical forward model are in function of environmental components such as the surface material composition and the antenna gain patterns. Hence, in order to assess this deficiency in the parameters it is necessary to apply corrections based on their optimal values using empirical biases. Thereby, the new forward model and its respective augmented parameters yields the following (Nievinski and Larson, 2014a):

$$P_d = P_d/K \quad (5)$$

$$\phi_i = \phi_i - \phi_B \quad (6)$$

$$P_i = P_i/B^2 \quad (7)$$

$$SNR = P_d(1 + P_i + 2\sqrt{P_i}\cos\phi_i)K/P_n \quad (8)$$

where B is a complex-valued interferometric bias in the form $B = |B|\exp(\sqrt{-1}\phi_B)$ which can be enhanced for the reflection power B_{dB} and phase ϕ_B bias as a polynomial form in function of $\sin e$, respectively. Similarly, the parameter K is a non-negative real-valued noise power bias represented in decibels and expanded as a polynomial in the form $K_{dB} = \sum_{j=0,1,\ldots} K_{dB}^{(j)} sin^j e$ (Nievinski and Larson, 2014a). The inverse model handles the physical model stated above to simulate SNR observations expecting no biases to compute corrections through a least-square procedure using the residuals between the measured and simulated observations. Thereby, it is necessary to estimate the linear coefficient phase bias $\phi_B^{(1)}$ which can be shifted into the corresponding reflector height bias as $H_B = \phi_B^{(1)}\lambda/4\pi$. Finally, the discrepancy between the pre-fit parameter $H^{'}$ and its equivalent post-fit bias H_B represents the total reflector height $H_T = H^{'} - H_B$ (Nievinski and Larson, 2014a).

3. Case study: The Sanalona dam

The Sanalona dam is located on the Tamazula riverbed at the municipality of Culiacan in northwestern Mexico and its geographic coordinates are near 24°48′51″N, 107° 09′05″W (See Fig. 4). The construction of the Sanalona dam began in 1941 and ended in early 1948. Fifteen years later, the hydroelectric power plant capable of generating 14 megawatts of electrical energy began to operate. The dam extends over 5420 ha and has a reservoir capacity of approximately 673 million cubic meters of water. The Sanalona dam is a gravity-type dam with rock-fill built mainly with hauled materials and reinforced concrete. The dam has a height of 81 m, a crest length and a width of 415 and 10 m, respectively. Currently, the Sanalona dam has been operating for 73 years, surpassing the structural period of life recommended by the National Water Commission in Mexico (CONAGUA, acronyms in Spanish). For this reason, in order to improve the dam structural performance CONAGUA carried out a rehabilitation process in the year 2020.

It is worth mentioning that SSIG station was not installed for GNSS-R water level purposes. Nonetheless, the site has characteristics that allow the application of the inversion GNSS-R technique. In this sense, the station has a clear view of the sky which implies that the receiver can record direct and reflected GPS signals. However, the geographical environment around the antenna (vegetation, rocks and dry soil on a tilted surface, since the station is over a hill) makes the GNSS-R process a real challenge. In order to assess this, we analyzed the measured and modeled SNR waveform computed from the forward and inverse model with the purpose of determine the best fit or quality multipath signal. Generally, best-fit SNR observations present a sinusoid form whose amplitude decrease as the elevation angle increases. In the present case study, the SNR signals originated in water were marked with a yellow outline in Fig. 5a. These signals exhibit a sinusoid form and its amplitude and increasing trend barely varies over the elevation angle (Fig. 5b and c). This pattern degradation is due to mainly two factors. First, to avoid utmost

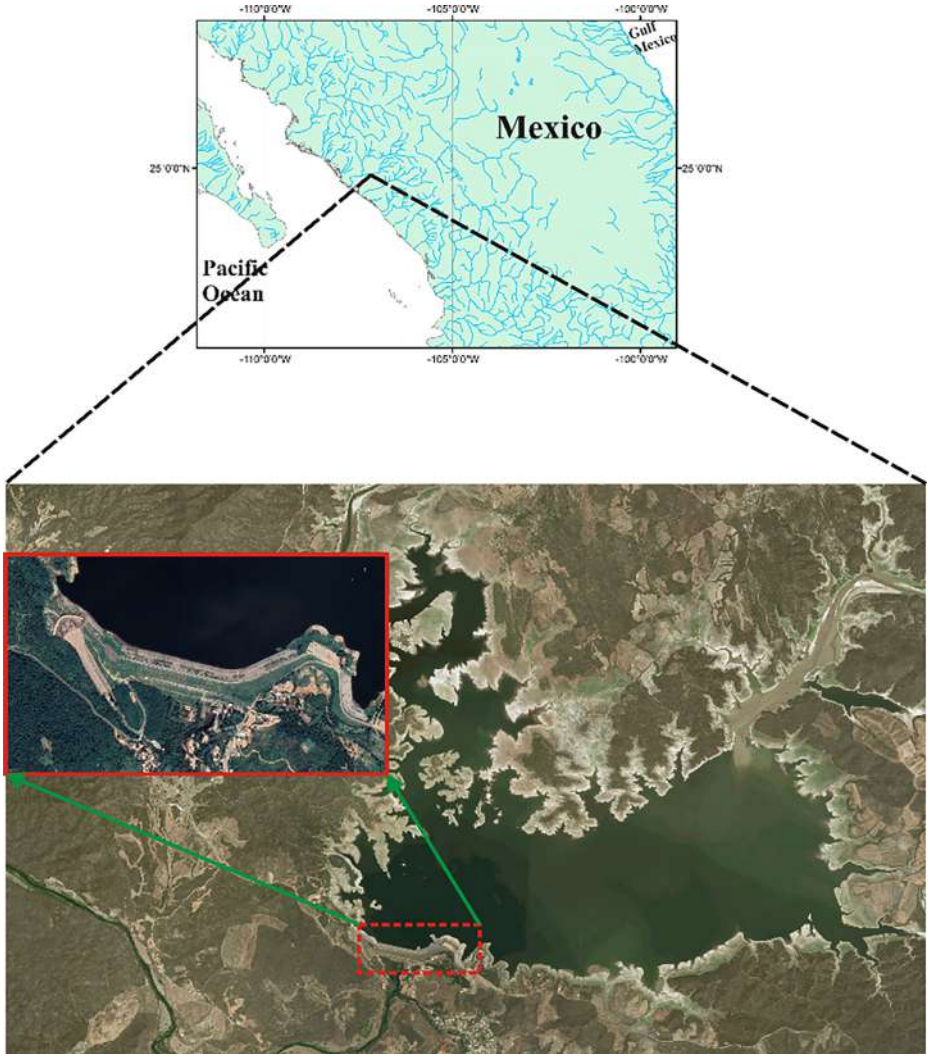

Fig. 4. Geographic location of the Sanalona dam.

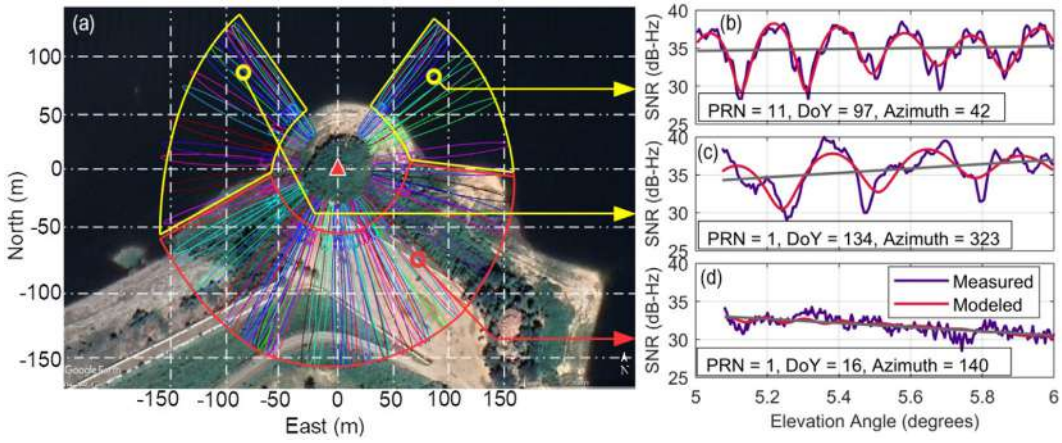

Fig. 5. (a) First Fresnel Zones (FFZ) of the SSIG station (red triangle) for a single day. (b) and (c) shows best-fit SNR samples from both azimuths mask in yellow with its respective trend (grey line) for the year 2018. (d) presents a deficient SNR sample from land-side azimuth in red (satellite image: Google Earth). (For interpretation of the references to colour in this figure legend, the reader is referred to the web version of this article.)

the solid terrain nearby the antenna, the modeled signal which is based on the measured SNR was shortened to one degree range. Therefore, it was not possible to observe the complete SNR sinusoid pattern. Second, since the height of the antenna phase center over the reflecting surface was relatively high (~8 m) the possibility of second

reflections interacting with the terrain before reaching the antenna was exposed.

On the other hand, as the multipath signals interact with different surface types, i,e., soil, rocks and vegetation, the sinusoid pattern changes, presenting random forms or atypical interference fringes (Fig. 5d). Hence, based on the SNR waveform analysis, we applied an observation mask dividing the sensing zone azimuth (see Fig. 5a) into two quadrants (0° to 90° and 270° to 360°) and limited the elevation angles from 5° to 6°. The sensing zone was composed in terms of the First Fresnel zones (FFZ), which are thin ellipses surrounding the antenna. The size of the FFZ is based on two parameters e and H, which corresponds to the elevation angle of the satellite with respect to the horizon and the height of the antenna above the reflecting planar surface, respectively. In addition, the FFZ position around the antenna is based on the satellite azimuth (Larson et al., 2017; Löfgren et al., 2011a,b), yet a portion at the north of the sensing zone without positioned FFZ was presented due to the GPS constellation orbital inclination. In this sense, the FFZ length changes as the satellite track advance over the sky. Then, when the satellite is setting on the horizon at low elevation angles the length is increased.

Otherwise, when the satellite is rising in the sky the length decrease. Fig. 5a illustrates the FFZ at SSIG station for the L1 C/A frequency ($f = 1,575.4MHz$, $\lambda = 19.05cm$) with different lengths due to elevation angles of 5° to 25° and its respective positions from azimuths of 0° to 360° with an antenna height of 8 m. The mask mentioned above guarantees that most reflected SNR observations come from the dam water. Nevertheless, the mask substantially reduces the number of valid SNR observations. Furthermore, in order to increase the number of recorded GPS signals we selected the GPS legacy civil L1 C/A signal, since it is transmitted by more satellites compared to other signals such as L2C and L5. Finally, the mean water level was subtracted from the reference time series and later added to the GNSS-R time series. The above in order to make the vertical datum consistent for both time series.

4. Results

4.1. Deformation of the sanalona dam

The results obtained after processing with GAMIT/GLOBK scientific software indicated the velocities in the three components (North, East, Up) of the SSIG station located on the crest of the Sanalona dam. Considering that rock-filled gravity-type dams are very rigid structures its displacements are usually very small (in the order of millimeters) (Acosta et al., 2018) and mainly consequence of hydrostatic thrust force. Therefore, the greatest displacements are expected to occur when the dam reach its maximum reservoir level.

The velocities presented in the Sanalona dam were -6.77 ± 0.08 mm/yr, -9.95 ± 0.06 mm/yr and -1.62 ± 0.18 mm/yr in components N, E and U, respectively. Fig. 6 shows the time series generated by GAMIT/GLOBK and edited with the tsview tool from the SSIG station for a measurement period corresponding to 3.519 years. Unfortunately, some data gaps can be observed. This was a

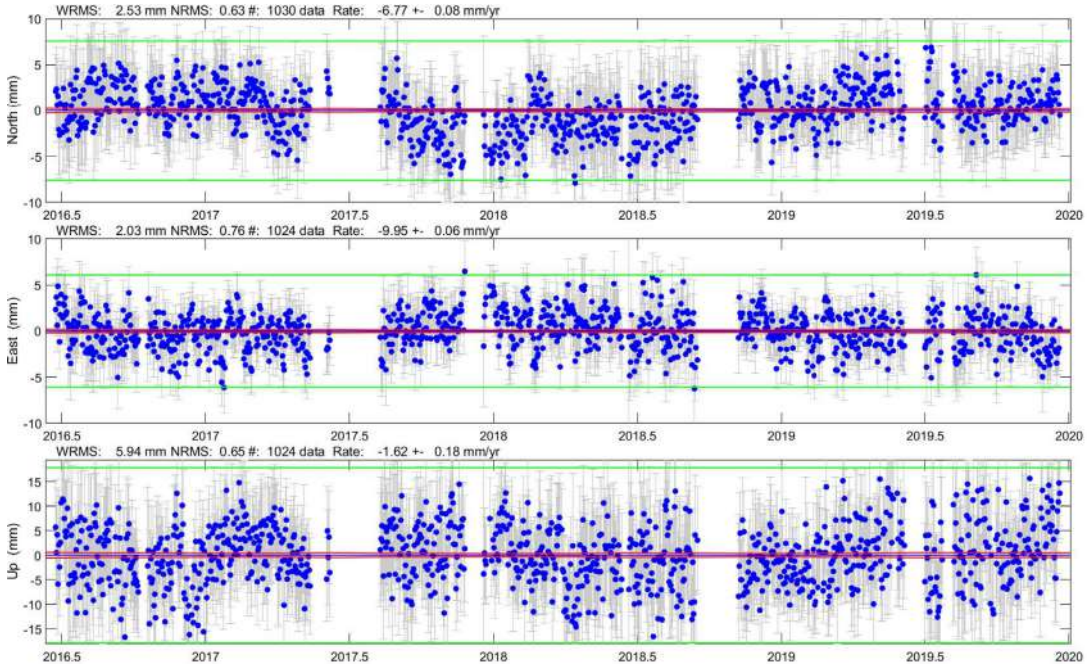

Fig. 6. Time series of the SSIG station for the three components (N, E, U). Blue dots: daily positions with respect to the reference position in its three NEU components. Red lines: correspond to the estimated realistic uncertainties ($\pm 1\sigma$). Green lines: weighted mean square error of each component in mm (± 3 of dispersion). (For interpretation of the references to colour in this figure legend, the reader is referred to the web version of this article.)

consequence of failures in the GPS receiver for such periods (the data was not uploaded correctly). However, the missing data corresponds to approximately less than 12% of the total data, a low percentage to affect the solutions generated by GAMIT/GLOBK.

The North and East components presented a lower dispersion compared to the Up component. The North component showed displacements in the order of ± 8 mm and for the East component of ± 6 mm. As mentioned above, the component that should present the greatest displacements is the one with the same direction of the thrust force. For this case, it was the North component, being the East component perpendicular to the pushing force of the water. Therefore, the effects of the thrust force were minor. This is demonstrated in Fig. 6.

4.2. Reservoir level of the Sanalona dam from GNSS-R

In addition, Fig. 7 illustrates the dam water level variations (DWL) in the Sanalona reference meteorologic station (DWLR) for a period of four years as well as the GNSS-R water level retrievals. It is worth mentioning that both instruments presented different measurement rates, e.g., GNSS-R was recording data at 1 Hz meanwhile the DWLR station recorded one data per day. However, the GNSS-R water level retrievals rely on the available rising and setting satellites, which are in the order of ~1 retrieval every hour. Furthermore, it was possible to appreciate multiple data gaps affecting the GNSS-R time series. This issue was a consequence of both the azimuth and elevation angle masks applied in the processing step and to missing data resulting from spontaneous environment factors which induce instrumentation malfunctions. Moreover, precipitation data for the same period were acquired and contrasted in conjunction with both time series. Based on this complementary information it was possible to appreciate the hydrological cycle of the study area. In particular, in Fig. 7 the rainfall measurements were indicated with filled yellow dots. Moreover, it was possible to observe how these dots started rising and scattering at the beginning of each time series peak. This indicated that rainfall seasons agreed with the increase of the DWL.

Besides, in order to evaluate the precision of the GNSS-R a correlation was performed and represented in a scatterplot (see Fig. 8). The aforementioned was done comparing the water level retrievals between the GNSS-R and the DWLR. In this instance, the majority of the points are positioned close to the regression line, with some scattered

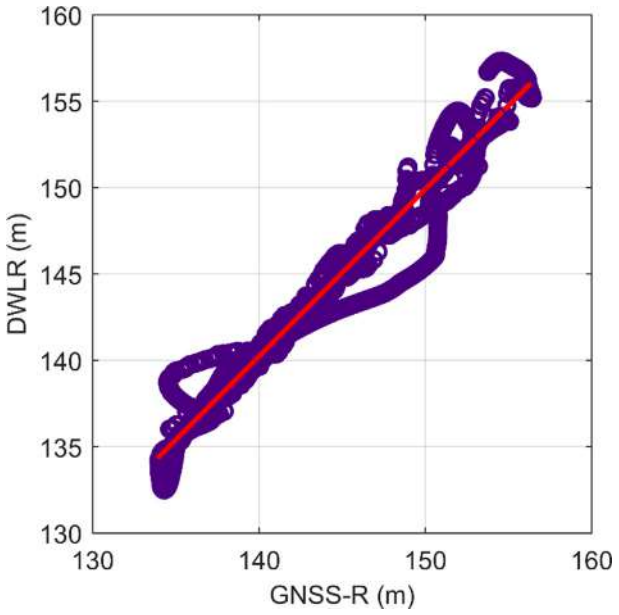

Fig. 8. Scatterplot plot between the GNSS-R and the DWLR measurements.

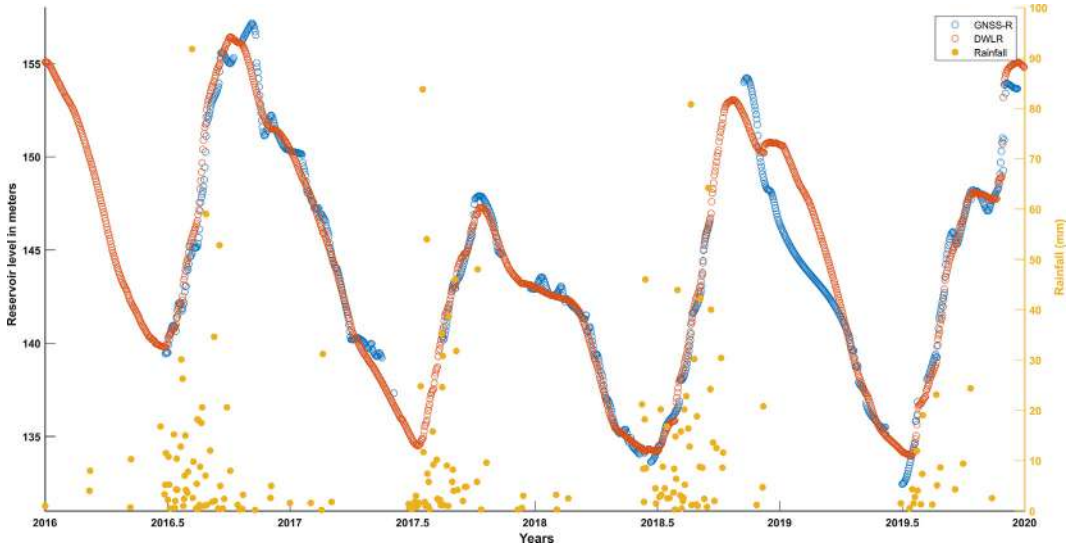

Fig. 7. Sanalona dam water level time series for the meteorologic reference station (DWLR) in orange and GNSS-R in blue circles, respectively. Precipitations for the same period are shown in yellow dots. (For interpretation of the references to colour in this figure legend, the reader is referred to the web version of this article.)

points placed on the lower-centered side of the regression. Moreover, a linear regression was applied in order to quantify systematic scale differences between both instruments. The GNSS-R achieved a correlation coefficient (ρ) of 0.97 with a root-mean-square error (RMSE) of 1.36 m and a regression slope of 0.932 m/m. The above indicated a good agreement between both DWL measurements.

With the objective of analyze the quality of the DWL measurements, we performed a Van de Casteele test (see Fig. 9). This test can be represented as a diagram that allows the identification of different types of systematics errors commonly presented in tide-gauge measurements as well as for validate new instrumentation dedicated to measure water level in function of a reference tide-gauge previously installed and validated (Miguez et al., 2008).

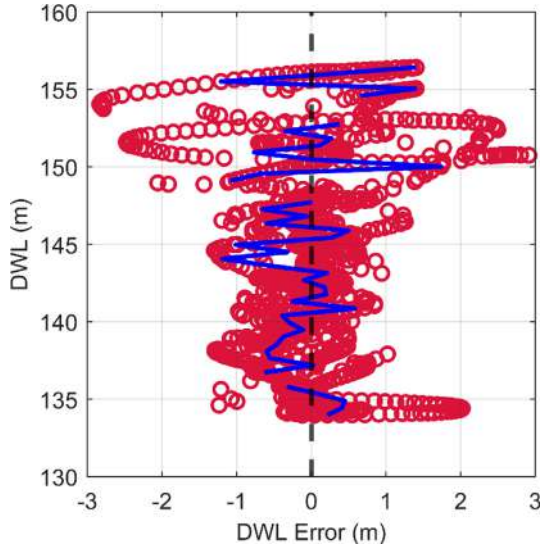

Fig. 9. Van de Casteele diagram between the GNSS-R water level retrievals and the reference time series (DWLR).

Based on previous studies, such as Larson et al., (2017) and Löfgren and Haas, (2014) the x-axis represents the discrepancy ΔH between the DWL measured by the GNSS-R and the reference time series. On the other hand, the y-axis describes the DWL obtained by means of both respective instruments. Accordingly, points are located around zero since we previously applied a regression to correct involved scale-based systematic errors. Therefore, the distribution and shape of the points across the diagram allowed the identification of significant and, in some cases, random systematic errors involved in the measurements, such as scale and time-shift errors, low performance, instrument malfunction, and others.

Based on Fig. 9, it is possible to notice that the red dots form a pseudo-symmetric shape across both sides of the vertical line centered at zero, suggesting that instrumental background noise was presented in the GNSS-R water level measurements. Moreover, the blue line represents the smoothed error based on a moving average (Geremia-Nievinski et al., 2020) and the gaps in the figure correspond to missing data resulting from the smoothing procedure. Nonetheless, it is possible to notice how data was scattered at high water levels and at both sides of the diagram. Conversely, a minor number of data dots were scattered on the positive low-right side of the diagram. This indicate that the performance of the GNSS-R was only negatively affected at high (>150 m) and low (<135 m) water levels.

4.3. Correlation of GPS deformation and reservoir level

A correlation analysis was carried out between the reservoir level of the dam and the displacements of the SSIG station in the three components. This, in order to find the impact of the reservoir level and its effects on the deformation of the crest of the Sanalona dam. For that purpose, the data obtained from the moving average filter were used

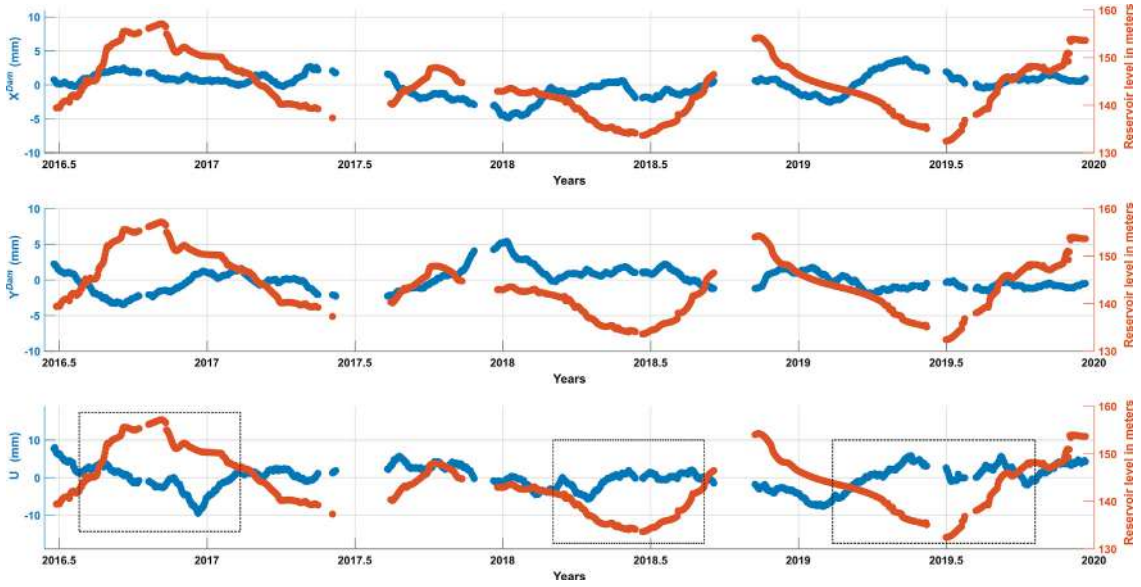

Fig. 10. Comparison between reservoir level calculated with GNSS-R and deformations in the three components (NEU) of the Sanlona dam.

(x^{Dam}, y^{Dam}, U). The results indicated a correlation between the reservoir level and the deformation of the dam in the three components (x^{Dam}, y^{Dam}, U). In the case of the x^{Dam} component a negative correlation was observed in the majority of the time series. In specific, when the displacements were negative the deformation of the dam was downstream and when the displacements were positive the deformation was upstream. Usually, when the reservoir level increase the downstream deformations are expected to increase but this is not always the case. The maximum downstream and upstream deformation for the x^{Dam} component was at the beginning of 2018 and 2019.5, respectively. Moreover, when the reservoir level was at its lower level the upstream deformation was greater; Thus, the structure of the dam presented elastic displacements, which were of the order of ±5 mm. On the other hand, the y^{Dam} component presented lower displacements. This because the thrust force did not have a great effect on y^{Dam}. However, the displacements showed in Fig. 10 were in the range of −3 mm and 5 mm. These displacements did not correlate with the thrust force and can be the consequence of other phenomena, for example horizontal hydrological loads on the dam which have less impact than the thrust force. For the case of the U component, it can be observed in Fig. 10 that when the reservoir level increased the structure descends and when the reservoir level decreased to its maximum the structure returns to its vertical origin (black boxes in Fig. 10 bottom-panel), where the maximum displacement of U was 1 cm. Variation in the vertical behavior of the dam can be generated due to two factors: first, solutions with low precision in the GAMIT/GLOBK processing and second, effects of the static pressure of the water which interacts with the surface of the dam.

5. Conclusions

In this study GPS data processing was carried out with the GAMIT/GLOBK scientific software and with the inverse modeling GNSS reflectometry (GNSS-R) technique in order to find three-dimensional displacements and the reservoir level over the Sanalona dam. The results indicated that the structure of the Sanalona dam was very rigid and presented small displacements, the latter is in concordance with the type of dam. The velocities found on the crest of the dam were −6.77 ± 0.08 mm/yr, −9.95 ± 0.06 mm/yr, and −1.62 ± 0.18 mm/yr in the N, E, and U components, respectively. The three-dimensional displacements of the Sanalona dam corresponding to the evaluation period (3.519 years) were approximately ±5 mm, ±4–5 mm, and ±10 mm for components x^{Dam}, y^{Dam} and U, respectively. The Up component presented the greatest displacement due to the possible local settlement of the dam caused by the vertical thrust force or the static pressure of the water. In the other components, x^{Dam} presented the greatest horizontal displacements on the dam crest where the reservoir level of the dam caused these displacements. For component y^{Dam}, it showed minor displacements on the dam curtain, mainly because the horizontal thrust force did not presented strong effects on it. The reservoir level caused elastic displacements on the dam crest where each component of the structure moved over an origin point. These displacements are not likely to be considered dangerous for the correct operation of the dam; Therefore, the structure can be considered secure due to the stability it presents even when it have exceeded its lifespan. On the other hand, we concluded that deformations on the crest of dams were the consequence of its reservoir level, since there was a strong correlation between them, mainly in the x^{Dam} and U component.

In addition, we enabled a GNSS station for water level monitoring purposes over a period of 3.5 years. However, due to the challenging environmental conditions surrounding the antenna, such as rocks, mixed dense vegetation, tilted surface, among others it was necessary to use two azimuth mask and decreased the elevation angle in a range of one degree in order to receive as many reflections as possible from the dam water under different levels. In contrast to the meteorologic reference station, the GNSS-R water level measurements obtained a high correlation of 0.97 with an RMSE of 1.36 m. Notwithstanding, a low precision in RMSE terms was found. The latter was a consequence of bad quality SNR signals affected by dry soil exposed over long periods, when the dam water level was low. Furthermore, the Van de Casteele test contrasted that random systematic errors were slightly lower when the water level was less than 150 m and higher than 135 m. Otherwise, these errors may increase, affecting negatively the GNSS-R performance. Nevertheless, although the water level monitoring through GNSS-R can not replace the meteorologic reference station in terms of precision, we concluded that this GNSS station can operate as a secondary measurement tool since the derived water level retrievals were consistent with the reference station. Accordingly, it was well-established that GPS technology is a powerful tool for monitoring slow displacements over long periods on structures such as dams.

Finally, in regards to GNSS and GNSS-R, we support its simultaneously use for the Structural Health Monitoring in gravity-type dams due to its capacity to detect settlement displacements and monitor the reservoir level which is the main cause of horizontal displacements in the dam's crest, respectively.

Declaration of Competing Interest

The authors declare that they have no known competing financial interests or personal relationships that could have appeared to influence the work reported in this paper.

Acknowledgments

"The seismological data were obtained by the National Seismological Service in Mexico. We are grateful to SSN

staff for the stations maintenance and the acquisition and distribution of data".

References

Acosta, L.E., De Lacy, M., Ramos, M.I., Cano, J.P., Herrera, A.M., Avilés, M., Gil, A.J., 2018. Displacements study of an earth fill dam based on high precision geodetic monitoring and numerical modeling. Sensors 18 (5), 1369. https://doi.org/10.3390/s18051369.

Alcay, S., Ogutcu, S., Kalayci, I., Yigit, C.O., 2019. Displacement monitoring performance of relative positioning and Precise Point Positioning (PPP) methods using simulation apparatus. Adv. Space Res. 63 (5), 1697–1707. https://doi.org/10.1016/j.asr.2018.11.003.

Bilich, A., Axelrad, P.M., Larson, K., 2007. Scientific utility of the signal-to-noise ratio (SNR) reported by geodetic GPS receivers. In: Proceedings of the 20th International Technical Meeting of the Satellite Division of The Institute of Navigation (ION GNSS 2007) 1999–2010.

Blewitt, G., Lavallée, D., 2002. Effect of annual signals on geodetic velocity. J. Geophys. Res.: Solid Earth 107 (B7), ETG 9-1–ETG 9-11. https://doi.org/10.1029/2001JB000570.

Bukenya, P., Moyo, P., Beushausen, H., Oosthuizen, C., 2014. Health monitoring of concrete dams: a literature review. J. Civil Struct. Health Monit. 4 (4), 235–244. https://doi.org/10.1007/s13349-014-0079-2.

Cipollini, P., Calafat, F.M., Jevrejeva, S., Melet, A., Prandi, P., 2017. Monitoring sea level in the coastal zone with satellite altimetry and tide gauges. Surv. Geophys. 38 (1), 33–57. https://doi.org/10.1007/s10712-016-9392-0.

Ehiorobo, J.O., Irughe-Ehigiator, R., 2011. Monitoring for horizontal movement in an earth dam using differential GPS. J. Emerg. Trends Eng. Appl. Sci. 2 (6), 908–913.

Estey, L.H., Meertens, C.M., 1999. TEQC: the multi-purpose toolkit for GPS/GLONASS data. GPS Solut. 3 (1), 42–49.

FEMA (Federal Emergency Management Agency), 2015. Federal guidelines for dam safety risk management. FEMA P-1025. Washington (DC): US Department of Homeland Security.

Geremia-Nievinski, F., Hobiger, T., Haas, R., Liu, W., Strandberg, J., Tabibi, S., Vey, S., Wickert, J., Williams, S., 2020. SNR-based GNSS reflectometry for coastal sea-level altimetry: results from the first IAG inter-comparison campaign. J. Geod. 94, 70. https://doi.org/10.1007/s00190-020-01387-3.

González-Aguilera, D., Gómez-Lahoz, J., Sánchez, J., 2008. A new approach for structural monitoring of large dams with a three-dimensional laser scanner. Sensors 8 (9), 5866–5883. https://doi.org/10.3390/s8095866.

Graham, W.J., 1999. A Procedure for Estimating Loss of Life Caused by Dam Failure (DSO-99-06). US Bureau of Reclamation, Denver CO, USA.

Guler, G., Kilic, H., Hosbas, G., Ozaydin, K., 2006. Evaluation of the movements of the dam embankments by means of geodetic and geotechnical methods. J. Surv. Eng. 132 (1), 31–39. https://doi.org/10.1061/(ASCE)0733-9453(2006)132:1(31).

Guzman-Acevedo, G.M., Vazquez-Becerra, G.E., Millan-Almaraz, J.R., Rodriguez-Lozoya, H.E., Reyes-Salazar, A., Gaxiola-Camacho, J.R., Martinez-Felix, C.A., 2019. GPS, accelerometer, and smartphone fused smart sensor for SHM on real-scale bridges. Adv. Civil Eng. 2019, 1–15. https://doi.org/10.1155/2019/6429430.

Herring, T., 2003. MATLAB Tools for viewing GPS velocities and time series. GPS Solut. 7 (3), 194–199. https://doi.org/10.1007/s10291-003-0068-0.

Herring, T.A., King, R.W., McClusky, S.C., 2010. Introduction to gamit/globk. Massachusetts Institute of Technology, Cambridge, Massachusetts.

Hudnut, K.W., Behr, J.A., 1998. Continuous GPS monitoring of structural deformation at Pacoima Dam, California. Seismol. Res. Lett. 69 (4), 299–308.

Joseph, A., 2010. What is the difference between SNR and C/N0? Inside GNSS 5, 20–25.

Kalkan, Y., 2014. Geodetic deformation monitoring of Ataturk Dam in Turkey. Arab. J. Geosci. 7 (1), 397–405. https://doi.org/10.1007/s12517-012-0765-5.

Konakoglu, B., Cakir, L., Yilmaz, V., 2020. Monitoring the deformation of a concrete dam: a case study on the Deriner Dam, Artvin, Turkey. Geomat. Natl. Hazards Risk 11 (1), 160–177. https://doi.org/10.1080/19475705.2020.1714755.

Larson, K.M., Löfgren, J.S., Haas, R., 2013. Coastal sea level measurements using a single geodetic GPS receiver. Adv. Space Res. 51 (8), 1301–1310. https://doi.org/10.1016/j.asr.2012.04.017.

Larson, K.M., Ray, R.D., Williams, S.D.P., 2017. A 10-year comparison of water levels measured with a geodetic GPS receiver versus a conventional tide gauge. J. Atmos. Oceanic Technol. 34, 295–307. https://doi.org/10.1175/JTECH-D-16-0101.1.

Löfgren, J.S., Haas, R., 2014. Sea level measurements using multi-frequency GPS and GLONASS observations. EURASIP J. Adv. Signal Process. 2014, 50. https://doi.org/10.1186/1687-6180-2014-50.

Löfgren, J.S., Haas, R., Johansson, J.M., 2011a. Monitoring coastal sea level using reflected GNSS signals. Adv. Space Res. 47 (2), 213–220. https://doi.org/10.1016/j.asr.2010.08.015.

Löfgren, J.S., Haas, R., Scherneck, H.-G., 2014. Sea level time series and ocean tide analysis from multipath signals at five GPS sites in different parts of the world. J. Geodyn. 80, 66–80. https://doi.org/10.1016/j.jog.2014.02.012.

Löfgren, J.S., Haas, R., Scherneck, H.-G., Bos, M.S., 2011b. Three months of local sea level derived from reflected GNSS signals. Radio Sci. 46. https://doi.org/10.1029/2011RS004693.

Miguez, B.M., Testut, L., Wöppelmann, G., 2008. The van de casteele test revisited: an efficient approach to tide gauge error characterization. J. Atmos. Oceanic Technol. 25, 1238–1244. https://doi.org/10.1175/2007JTECHO554.1.

Munyaneza, O., Wali, U.G., Uhlenbrook, S., Maskey, S., Mlotha, M.J., 2009. Water level monitoring using radar remote sensing data: application to Lake Kivu, central Africa. Phys. Chem. Earth Parts A/B/C 34 (13–16), 722–728. https://doi.org/10.1016/j.pce.2009.06.008.

Nievinski, F.G., Larson, K.M., 2014a. Inverse modeling of GPS multipath for snow depth estimation—Part I: Formulation and simulations. IEEE Trans. Geosci. Remote Sens. 52 (10), 6555–6563. https://doi.org/10.1109/TGRS.2013.2297681.

Nievinski, F.G., Larson, K.M., 2014b. Inverse modeling of GPS multipath for snow depth estimation—Part II: Application and validation. IEEE Trans. Geosci. Remote Sens. 52 (10), 6564–6573. https://doi.org/10.1109/TGRS.2013.2297688.

Pytharouli, S.I., Stiros, S.C., 2005. Ladon dam (Greece) deformation and reservoir level fluctuations: evidence for a causative relationship from the spectral analysis of a geodetic monitoring record. Eng. Struct. 27 (3), 361–370. https://doi.org/10.1016/j.engstruct.2004.10.012.

Ridolfi, E., Manciola, P., 2018. Water level measurements from drones: a pilot case study at a dam site. Water 10 (3), 297. https://doi.org/10.3390/w10030297.

Song, M., He, X., Wang, X., Zhou, Y., Xu, X., 2019. Study on the quality control for periodogram in the determination of water level using the GNSS-IR technique. Sensors 19 (20), 4524. https://doi.org/10.3390/s19204524.

Soulat, F., Caparrini, M., Germain, O., Lopez-Dekker, P., Taani, M., Ruffini, G., 2004. Sea state monitoring using coastal GNSS-R: sea state monitoring using GNSS-R. Geophys. Res. Lett. 31 (21), n/a–n/a. https://doi.org/10.1029/2004GL020680.

Strandberg, J., Hobiger, T., Haas, R., 2016. Improving GNSS-R sea level determination through inverse modeling of SNR data: GNSS-R inverse modeling. Radio Sci. 51 (8), 1286–1296. https://doi.org/10.1002/rds.v51.810.1002/2016RS006057.

Tabibi, S., Geremia-Nievinski, F., van Dam, Tonie, 2017. Statistical comparison and combination of GPS, GLONASS, and multi-GNSS multipath reflectometry applied to snow depth retrieval. IEEE Trans.

Geosci. Remote Sens. 55 (7), 3773–3785. https://doi.org/10.1109/TGRS.2017.2679899.

Vazquez-Ontiveros, J.R., Vazquez-Becerra, G.E., Quintana, J.A., Carrion, F.J., Guzman-Acevedo, G.M., Gaxiola-Camacho, J.R., 2021. Implementation of PPP-GNSS measurement technology in the probabilistic SHM of bridge structures. Measurement 173, 108677. https://doi.org/10.1016/j.measurement.2020.108677.

Xi, R., Zhou, X., Jiang, W., Chen, Q., 2018. Simultaneous estimation of dam displacements and reservoir level variation from GPS measurements. Measurement 122, 247–256. https://doi.org/10.1016/j.measurement.2018.03.036.

Xiao, R., Shi, H., He, X., Li, Z., Jia, D., Yang, Z., 2019. Deformation monitoring of reservoir dams using GNSS: an application to south-to-north water diversion project, China. IEEE Access 7, 54981–54992. https://doi.org/10.1109/Access.628763910.1109/ACCESS.2019.2912143.

Yang, L., Liu, M., Smith, J.A., Tian, F., 2017. Typhoon nina and the August 1975 flood over central China. J. Hydrometeorol. 18 (2), 451–472. https://doi.org/10.1175/JHM-D-16-0152.1.

Yavaşoğlu, H.H., Kalkan, Y., Tiryakioğlu, İ., Yigit, C.O., Özbey, V., Alkan, M.N., Bilgi, S., Alkan, R.M., 2018. Monitoring the deformation and strain analysis on the Ataturk Dam, Turkey. Geomat. Natl. Hazards Risk 9 (1), 94–107. https://doi.org/10.1080/19475705.2017.1411400.

Yigit, C.O., Alcay, S., Ceylan, A., 2016. Displacement response of a concrete arch dam to seasonal temperature fluctuations and reservoir level rise during the first filling period: evidence from geodetic data. Geomat. Natl. Hazards Risk 7 (4), 1489–1505. https://doi.org/10.1080/19475705.2015.1047902.

Yigit, C.O., 2016. Experimental assessment of post-processed kinematic precise point positioning method for structural health monitoring. Geomat. Natl. Hazards Risk 7 (1), 360–383. https://doi.org/10.1080/19475705.2014.917724.